AGU ADVANCING EARTH AND SPACE SCIENCE

Geophysical Research Letters

RESEARCH LETTER
10.1029/2020GL089533

Zonal Asymmetry of the QBO Temperature Signal in the Tropical Tropopause Region

Susann Tegtmeier[1], James Anstey[2], Sean Davis[3], Ioana Ivanciu[4], Yue Jia[1], David McPhee[1], and Robin Pilch Kedzierski[4]

[1]Institute of Space and Atmospheric Studies, University of Saskatchewan, Saskatoon, Saskatchewan, Canada, [2]Canadian Centre for Climate Modelling and Analysis, Environment and Climate Change Canada, Victoria, British Columbia, Canada, [3]NOAA Chemical Sciences Laboratory, Boulder, CO, USA, [4]GEOMAR Helmholtz Centre for Ocean Research Kiel, Kiel, Germany

Key Points:
- QBO temperature signals in the tropical tropopause layer are enhanced over regions of high-reaching convection
- Zonal asymmetry of QBO signal is due to colder QBO cold phases over the convective regions
- Analysis suggests a positive feedback mechanism that amplifies the QBO cold phase temperature anomalies over convectively active regions

Supporting Information:
- Supporting Information S1

Correspondence to:
S. Tegtmeier,
susann.tegtmeier@usask.ca

Citation:
Tegtmeier, S., Anstey, J., Davis, S., Ivanciu, I., Jia, Y., McPhee, D., et al. (2020). Zonal asymmetry of the QBO temperature signal in the tropical tropopause region. *Geophysical Research Letters*, *47*, e2020GL089533. https://doi.org/10.1029/2020GL089533

Received 26 JUN 2020
Accepted 1 NOV 2020
Accepted article online 20 NOV 2020

Abstract The quasi-biennial oscillation (QBO) of the equatorial zonal wind leads to zonally symmetric temperature variations in the stratosphere that descend downward. Here we investigate the QBO-induced temperature anomalies in the tropical tropopause layer (TTL) and detect pronounced longitudinal variations of the signal. In addition, the QBO temperature anomalies show a strong seasonal variability. The magnitude of these seasonal and longitudinal QBO variations is comparable to the magnitude of the well-known zonal mean QBO signal in the TTL. At the cold point tropopause, the strongest QBO variations of around ±1.6 K are found over regions of active convection such as the West Pacific and Africa during boreal winter. The weakest QBO variations of ±0.25 K are detected over the East Pacific during boreal summer, while the zonal mean signal ranges around ±0.7 K. The longitudinal variations are associated with enhanced convective activity that occurs during QBO cold phases and locally enhances the cold anomalies.

Plain Language Summary Temperatures in the tropical stratosphere, the atmospheric region between 20°S and 20°N and above 18 km, oscillate between colder and warmer conditions with a full cycle taking about 28 months on average. Observations over the last decades have shown that the strength of this so-called quasi-biennial oscillation of stratospheric temperature is similar for all longitudes within the tropics. The temperature variations extend downward into the region that connects the stratosphere with troposphere. We show that in this transition region between the two atmospheric layers, the temperature oscillations can be stronger or weaker depending on the geographical position along the equator. Especially strong temperature oscillations are found over regions of frequently occurring thunderstorms such as the West Pacific and Africa. The fact that a stratospheric signal such as the quasi-biennial oscillation is linked with thunderstorms has implications for understanding how the upper atmosphere can impact tropical weather phenomena.

1. Introduction

The tropical tropopause layer (TTL) is the main gateway for air entering the stratosphere and sets the boundary conditions for stratospheric chemistry and composition (e.g., Fueglistaler et al., 2011; Holton & Gettelman, 2001). As the transition region between the turbulent, moist troposphere, and the stable, dry stratosphere, the TTL shows pronounced changes, not only in the vertical temperature structure but also in the distributions of atmospheric trace gases and clouds (e.g., Pan et al., 2018). The cold point tropopause (CPT) is defined as the level at which the vertical temperature profile reaches its minimum (Highwood & Hoskins, 1998). Air parcels en route from the troposphere to the stratosphere often encounter their final dehydration at the CPT. As a result, the CPT temperatures effectively control lower stratospheric water vapor (e.g., Fueglistaler et al., 2009), which can have a significant impact on climate (Solomon et al., 2010).

Upper tropospheric temperatures are mainly determined by large-scale radiative-convective equilibrium with persistent strong convection over continents and the western Pacific Ocean. Globally, they exhibit a small annual cycle but have large interannual variations in the tropics linked to the El Niño–Southern Oscillation (ENSO; Yulaeva & Wallace, 1994). In contrast, lower stratospheric temperatures are influenced by the Brewer Dobson circulation (BDC) with large-scale upwelling maintaining temperatures well below

radiative equilibrium. They are characterized by a distinct annual cycle along with large interannual changes linked to the quasi-biennial oscillation (QBO; Baldwin et al., 2001). Due to thermal wind balance, the temperature extremes occur directly in between the QBO east and west phases (Baldwin et al., 2001) with westerly wind shear leading to reduced upwelling and warm anomalies, while easterly wind shear causes cold anomalies (Plumb & Bell, 1982).

The TTL extends from the region of strong convective outflow near 12–14 km to the highest altitudes reached by convective overshooting events, around 18 km (e.g., Folkins et al., 1999). TTL temperatures are influenced by tropospheric and stratospheric processes, and their interannual variability is driven by BDC upwelling and large-scale modes such as ENSO and QBO (Randel & Wu, 2015). The negative phase of ENSO (i.e., La Niña) leads to enhanced deep convection over the tropical west Pacific with TTL cold anomalies directly above (Gettelman et al., 2001). During the positive phase (El Niño), similar cold anomalies occur over the central Pacific. In contrast, the QBO manifests as zonally uniform wind and temperature anomalies that descend through the tropical stratosphere down to the upper TTL. The QBO temperature signal in the TTL is relatively small (±0.5 K at the CPT) compared to the corresponding stratospheric variations (±4 K at 25 km) and maximizes between 10°S to 10°N (e.g., Randel & Wu, 2015). In general, the QBO is zonally symmetric, however, studies have suggested some longitudinal variations in middle stratospheric temperature (Patel et al., 2019) and wind (Hamilton et al., 2004).

Although the QBO is a stratospheric phenomenon, observational and modeling studies have shown that the descending QBO wind and temperature anomalies can impact tropical convection, precipitation and near-tropopause cirrus clouds (Davis et al., 2013). Seasonal mean deep convection over the western Pacific was found to be enhanced if the QBO easterly phase occurs during boreal winter (Collimore et al., 2003; Liess & Geller, 2012). In addition, interannual variations of subseasonal convective activity are significantly modulated by the QBO with an enhanced Madden–Julian oscillation (MJO) during the QBO easterly phase in boreal winter (e.g., Son et al., 2017). While the exact mechanisms of the connection between QBO and convection are unclear, it is believed that they are linked to QBO modulations of temperature, zonal wind shear and static stability around the tropical tropopause (e.g., Gray et al., 1992).

In this paper, we investigate the nature of the QBO temperature variations in the TTL including newly detected longitudinal variations of the signal. We are able to explain these variations by linking enhanced convective activity during QBO cold phases with intensified cold temperature anomalies over the convective regions. Results are presented in section 3, while data and methods are introduced in section 2.

2. Data and Methods

High-resolution temperature data in the TTL are available from satellite retrievals based on the Global Navigation Satellite System-Radio Occultation (GNSS-RO) technique. We use a monthly mean, gridded data set of cold point and 100 hPa temperatures constructed from measurements obtained from all major GNSS-RO missions between 2002 and 2018 (Pilch Kedzierski et al., 2020). For each profile, the CPT temperature was identified based on the cold point criteria and monthly mean profiles are computed for 30° × 10° bins between 30°N and 30°S (see Tegtmeier et al., 2020, for details).

Observations of the tropopause temperatures are also available from tropical radiosonde stations. Here, we use a monthly mean, gridded data set of 100 hPa temperatures based on the unadjusted, quality-controlled IGRA2 radiosondes (Durre et al., 2016). In addition, we use 100 hPa temperature records from five modern reanalyses, including the European Centre for Medium-Range Weather Forecasts (ECMWF) Interim Reanalysis (ERA-Interim; Dee et al., 2011) and ERA5 reanalysis (Hersbach et al., 2018), the Japanese 55-year Reanalysis (JRA-55; Kobayashi et al., 2015), the Modern Era Retrospective-Analysis for Research 2 (MERRA-2; Gelaro et al., 2017), and the Global Forecast System of the NCEP Reanalysis (CFSR; Saha et al., 2010).

The QBO temperature signal is calculated with a standard multivariate regression analysis:

$$T(t) = A_1 \cdot \mathrm{QBO1}(t) + A_2 \cdot \mathrm{QBO2}(t) + B \cdot \mathrm{ENSO}(t) + D \cdot \mathrm{VOL}(t). \quad (1)$$

QBO1(t) and QBO2(t) are orthogonal time series representing QBO variations constructed as the first two EOFs of the Freie Universität Berlin (FUB) radiosonde winds (Naujokat, 1986; Wallace et al., 1993).

ENSO(t) is the multivariate ENSO index (https://www.esrl.noaa.gov/psd/enso/mei/) and VOL(t) is the stratospheric aerosol optical depth from the Global Space-based Stratospheric Aerosol Climatology (Thomason et al., 2018).

The regression analysis is applied to the 100 hPa and the cold point time series of deseasonalized monthly temperature anomalies. The standard error of the regression coefficients is derived based on the bootstrap method (Efron & Tibshirani, 1993) and significance is tested based on a two-tailed test with a 99% confidence interval. The QBO temperature amplitude is calculated as the difference between the averaged maxima and averaged minima values of the QBO temperature fit time series $A_1 \cdot \mathrm{QBO1}(t) + A_2 \cdot \mathrm{QBO2}(t)$ (i.e., one maximum and one minimum value per QBO cycle).

Estimates of convective cloud occurrence are derived from geostationary infrared satellite imagery and microwave rainfall measurements (Pfister et al., 2001). We evaluate cloud top height within 0.5 km wide vertical bins to estimate the convective cloud occurrence frequency. Input data are given on a $0.25° \times 0.25°$ grid at a temporal resolution of 3 h for the period from 2005 to 2016. Convective cloud occurrence frequencies in the TTL are averaged to give monthly means on a $5° \times 5°$ grid and are taken to be an indicator of convective influence.

We use the daily outgoing longwave radiation (OLR)-based MJO index (OMI) (http://www.esrl.noaa.gov/psd/mjo/mjoindex/) to compute a monthly mean OMI amplitude. The daily OMI amplitude is based on the two principal component time series constructed from the 20–96 day band-pass-filtered OLR projected onto the two leading empirical orthogonal functions of the 30–96 day eastward filtered OLR (Kiladis et al., 2014).

3. Results

In the stratosphere, the impact of the QBO on interannual temperature variations is a zonally uniform signal. In the TTL, the zonal mean temperature variations associated with the QBO are relatively small, showing values of $\pm$0.4 K at 100 hPa (Tegtmeier et al., 2020) and quickly reaching zero at levels below (Randel & Wu, 2015).

We investigate if the QBO temperature variations in the TTL are a zonally uniform signal as is the case for the stratosphere. The impact of the QBO on temperature variations is presented as the amplitude of the QBO term derived from the multilinear regression analyses of the meridionally and zonally varying GNSS-RO, radiosonde and reanalysis data sets (Figure 1). All data sets show the strongest temperature response in the inner tropics (10°S to 10°N) with a QBO amplitude of up to 1.3 K, corresponding to variations of $\pm$0.65 K.

The QBO signal also shows pronounced variations with longitude (Table S1 in the supporting information), with the largest amplitude found over Central Africa (GNSS-RO), the western Indian Ocean to Maritime Continent (IGRA), or both of these regions (reanalyses). All data sets show relatively similar patterns and agree on the fact that the QBO variations in the Eastern Hemisphere are stronger than in the Western Hemisphere. In particular, regions known for cold anomalies associated with high-reaching convection (e.g., Liu & Liu, 2016) and Kelvin wave activity (Kim & Son, 2012), as listed above, show higher QBO variations, roughly twice as large as in other regions.

The data sets disagree on the exact location and magnitude of the maximum QBO signal. Some of these differences can be expected to arise from the data sets covering different time periods. Sensitivity tests (Figure S1) demonstrate that the QBO amplitude can vary up to a factor of two when shifting or shortening the analyzed time period. In addition, radiosonde data unevenly sample the tropics with higher station density over Maritime Continent than over Africa and the Atlantic (Wang et al., 2012).

The synoptic scale QBO variations also exist at the levels directly above 100 hPa such as the CPT (Figure 2a). Here, the zonal mean QBO amplitude is 1.4 K, corresponding to variations of $\pm$0.7 K. In the zonally resolved picture, the largest QBO signals of up to 1.9 K are found over Central Africa, the Indian Ocean and the Maritime Continent, similar to the QBO pattern at 100 hPa. The QBO signal minimizes over the central Pacific with an amplitude smaller than 1 K. The synoptic variations in QBO amplitude decrease with increasing altitude. While the zonal variability (expressed as the relative standard deviation of the QBO amplitude along the equator) is around 20% at the cold point, it is less than 5% at the 70 hPa level.

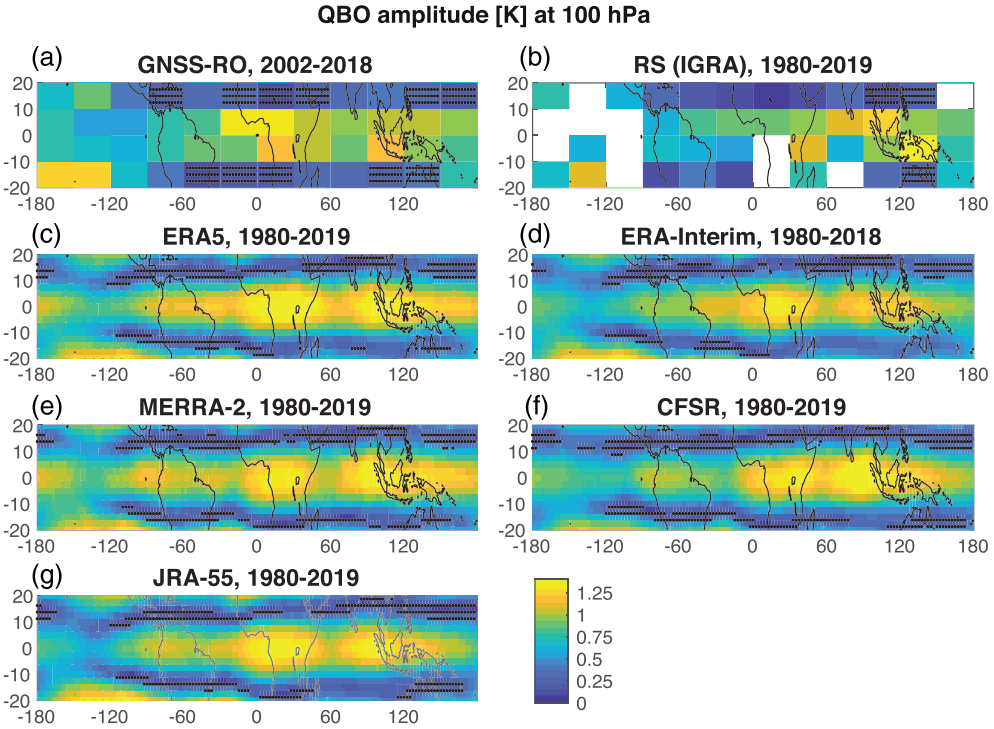

Figure 1. QBO amplitude at 100 hPa for GNSS-RO for 2002–2018 (a), IGRA radiosonde data for 1980–2019 (b) and five reanalyses for 1980–2018/19 (c–g). Stippling indicates regions with less than 99% statistical significance.

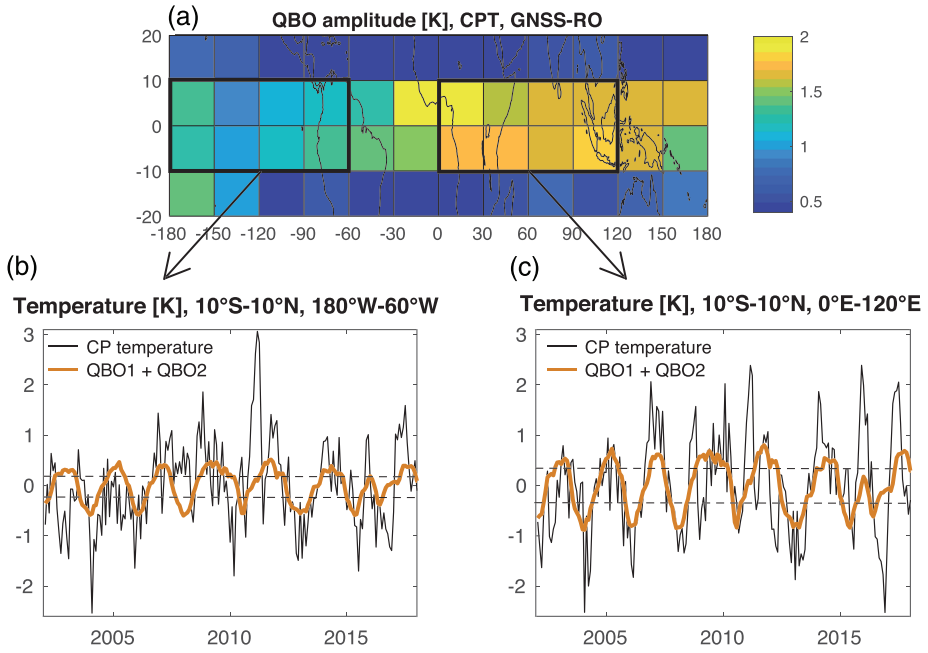

Figure 2. QBO amplitude at the cold point tropopause (CPT) for GNSS-RO for 2002–2018 (a). Deseasonalized CPT temperature anomalies and QBO fit for inner tropics 180–60°W (b) and 0–120°E (c). Dashed lines mark the levels of ±0.25 times the amplitude of the QBO fits.

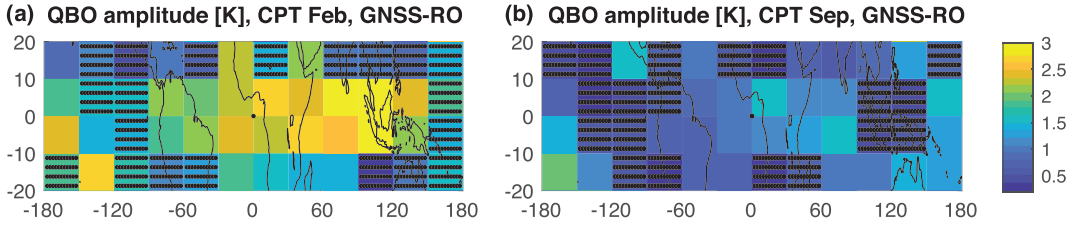

Figure 3. QBO amplitude at the cold point tropopause (CPT) for GNSS-RO for February (a) and September (b) of 2002–2018. Stippling indicates regions with less than 95% statistical significance.

We average the CPT temperature over two boxes in the inner tropics: 10°S to 10°N, 180–60°W (Figure 2b), and 10°S to 10°N, 0–120°E (Figure 2c), referred to hereinafter as the western and eastern tropics, respectively. The time series of deseasonalized CPT temperatures demonstrate that both regions exhibit variability of similar magnitude and timescale, but distinct QBO signals. The eastern tropics display clearer QBO variations (Figure 2c) resulting in the larger amplitude of the QBO temperature fit discussed earlier, while the phase of the signal is similar in both regions.

Previous studies have found seasonal variations in the coupling of tropical convection and the QBO. In order to analyze if such seasonal variations are also present in the QBO temperature patterns, we carry out the multilinear regression for 12 individual GNSS-RO temperature time series corresponding to the 12 months of the year. The QBO temperature amplitude for February and September (Figure 3) represents the strongest differences between boreal winter and summer. In February, the strength of the QBO signal is considerably larger and at the same time the synoptic scale variations are more pronounced. The amplitude of the February zonal mean QBO signal (2 K) is not only larger than the September amplitude (0.9 K) but also larger than the amplitude of the complete time series (1.4 K). During boreal winter, peak QBO variations are found over the Maritime Continent (3.2 K in February; Figure 3a) and Africa (3.1 K in January; Figure S2), while the QBO signals over the Eastern Pacific are considerably lower. The QBO variations during September, on the other hand, show only weak synoptic scale variations (Figure 3b). Regression patterns derived for other months confirm stronger QBO signals and larger synoptic variations from January to May and weaker signal with less pronounced variations during June–December.

The longitudinal differences of the QBO signal can lead to differences in the vertical temperature structure. In order to investigate the temperature profiles in different regions and QBO phases, we composite the eastern and western tropical GNSS-RO profiles according to QBO warm and cold phases. Since the QBO amplitude is determined by the maximum and minimum of each cycle, we aim to only include temperature profiles during peak QBO warm and cold conditions. We choose as a criterion that the QBO temperature fit must be warmer than one fourth of the QBO amplitude (upper dashed lines in Figures 2b and 2c) for the temperature profile to be grouped into QBO warm phase (24% of all profiles). Similarly, if the QBO temperature fit is colder than one fourth of the QBO amplitude (lower dashed lines in Figures 2b and 2c), the temperature profiles are grouped into QBO cold phase (26% of all profiles). Note that a QBO cold phase at around 100 hPa in general corresponds to a QBO easterly phase at around 50 hPa. Significance of the temperature differences between the two QBO phases is given as the 95% confidence interval obtained with the bootstrap method.

The profile comparison of the two QBO phases confirms that QBO-induced temperature variations are larger in the eastern tropics and demonstrates that they extend deeper into the upper troposphere (Figures 4a and 4b). While in the western tropics, there are no statistically significant differences between QBO cold and warm phase temperatures at altitudes below 80 hPa (~18 km), in the eastern hemisphere significant differences extend down to 130 hPa (~15 km).

Rearranging the profiles so that for each QBO phase the two regions can be compared directly reveals that there are no systematic longitudinal differences during the QBO warm phase with the eastern and western tropics showing nearly identical temperature profiles (Figure 4c). In contrast, during the QBO cold phase temperatures are considerably colder in the eastern tropics. Differences maximize between 120 and 90 hPa with temperatures in the eastern tropics being around 0.7 K lower than the western tropics. QBO

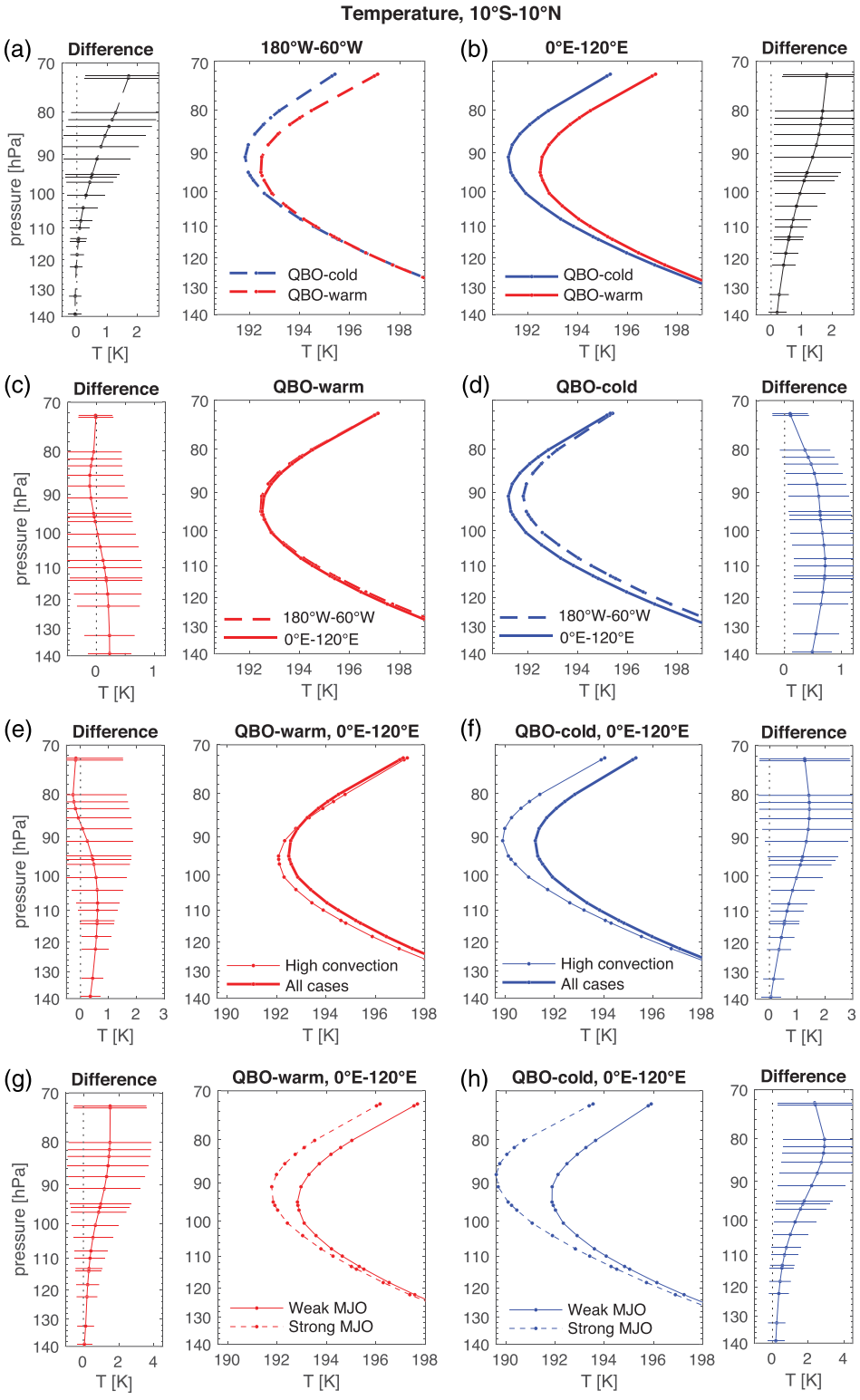

Figure 4. Composite of GNSS-RO temperature profiles according QBO warm and cold phases as defined in the text for the inner tropics (10°S to 10°N) at 180–60°W (a) and 0–120°E (b). Temperature profiles averaged over the two regions for QBO warm (c) and cold (d) phases. Eastern tropical temperature profiles averaged over all conditions and high convection only for QBO warm (e) and cold (f) phases and over weak and strong MJO conditions for QBO warm (g) and cold (h) phases. All profiles are shown in the inner panels and the respective differences with their 95% confidence intervals in the outer panels.

cold phase differences between the two regions are significant at all levels below 85 hPa. At the very upper levels shown here at around 70 hPa, temperature values in both regions are very similar and thus the longitudinal QBO variations are much smaller.

We aim to identify the conditions under which the QBO-induced temperature differences maximize. As the QBO signal penetrates deeper into the upper troposphere in the Eastern Hemisphere (Figure 4b), we test whether deep convection is associated with the enhanced signal in this region. Therefore, we use the convective cloud occurrence frequency between 14.5 and 17 km to composite the data further into time periods of high convective activity. Conditions are classified as "high convection" if the cloud occurrence frequency at a given time is higher than the long-term mean value (2005–2016) plus 0.7 times the standard deviation. For the chosen criterion, high convection occurs in the eastern tropics in 25% of all cases. The analysis discussed below shows similar but less pronounced results when using 0.5 times the standard deviation as the cut off level for identifying periods of high convective activity.

From the data used for the QBO warm and QBO cold profiles in the eastern tropics (Figure 4b), all profiles occurring during time periods of high convective activity are averaged ("high convection") and shown together with the profiles averaged over all convective conditions ("all cases") in Figures 4e and 4f. As expected, the comparison demonstrates that during both QBO phases, deep convection acts to reduce the temperature. However, for the QBO warm phase these differences are only significant at the lowest levels below 120 hPa. During QBO cold phases, on the other hand, the impact of high convective activity extends further upward causing additional cooling in the upper TTL (e.g., 1.2 K at 95 hPa). Differences are significant up to 95 hPa suggesting that deep convection-induced cooling is enhanced in the Eastern Hemisphere upper TTL during the QBO cold phase.

The same mechanism can also be expected to impact convective centers over the Western Hemisphere as indicated by slightly enhanced QBO amplitudes over South America (Figure 1). However, overall convective activity is less strong over the Western Hemisphere (e.g., Liu & Zipser, 2005). Furthermore, the tropopause region over South America has a higher stability than convective centers in the Eastern Hemisphere thus being less susceptible to convective penetration (Gettelman et al., 2002), consistent with a weaker impact of convection on the QBO.

In addition to the overall convective activity, we have composited the Eastern Hemisphere temperature profiles according to the MJO index (based on mean value $\pm$0.5 times the standard deviation). In general, the organized tropical convection associated with the MJO leads to lower TTL temperatures during both QBO phases (Figures 4g and 4h). As the MJO is enhanced during the QBO cold phase, the additional MJO induced cooling is stronger during the cold phase than during the warm phase resulting in amplified temperature variations over the Eastern Hemisphere.

4. Discussion and Summary

The QBO temperature signal shows pronounced longitudinal variations with the largest amplitudes found over Central Africa and the Maritime Continent. In particular, regions known for cold anomalies associated with high-reaching convection show stronger QBO signals, sometimes up to twice as large. The longitudinal variations of the QBO temperature signal maximize between 90 and 110 hPa and decrease above and below these levels. At the CPT, strongest QBO signals of around $\pm$1.6 K are found over the West Pacific and Africa during boreal winter. Weakest QBO variations of $\pm$0.25 K are detected over the East Pacific during boreal summer, while the zonal mean signal ranges around $\pm$0.7 K.

Composite temperature profiles indicate that the zonal asymmetries mostly result from anomalies during the QBO cold phase. While both regions show nearly identical QBO warm phase temperature profiles, considerable differences exist during the QBO cold phase with colder temperatures (1 K) over the eastern tropics. This additional cooling is associated with enhanced convective activities and a stronger MJO index during QBO cold conditions.

Earlier studies reported that the QBO east phase in the lower stratosphere (corresponding to a QBO cold phase in the TTL) favors reduced outgoing longwave radiation and more extensive deep convection over Amazonia, Africa, and Indonesia (e.g., Collimore et al., 1998; Knaff, 1993). The QBO was also suggested to have effects on tropical weather phenomena such as rainfall, cyclones, and the Walker circulation

(e.g., Camargo & Sobel, 2010; Gray et al., 1992; Yasunari, 1989). Mechanisms that link the QBO to deep tropical convection have been hypothesized to be related to the impact of temperature on thermodynamic efficiency of deep convection (Emanuel, 1997), vertical wind shear and dynamic disruptions (e.g., Gray et al., 1992), and inertial stability (Giorgetta et al., 1999).

Enhanced deep convection during the QBO cold phase, found in previous studies, can be expected to lead to an additional cooling in the TTL. This additional cooling will manifest itself in amplified negative temperature anomalies of the cold phase. Consistent with this, our study shows negative temperature anomalies during QBO cold phases over areas of deep convection (Figures 4c and 4d), which are particularly pronounced during time periods of strong convection (Figures 4e and 4f) or stronger MJO activity (Figures 4g and 4h). This amplification of the QBO cold phase over regions of high-reaching convection leads to the longitudinal variations of QBO signal detected in observations and reanalysis data (Figure 1). As the enhanced QBO signal is most likely caused by additional convective cooling, it can also be expected to extend further down into the TTL as confirmed by observational evidence (Figures 4a and 4b).

Stronger seasonal-mean and subseasonal deep convection over the western Pacific for the QBO easterly phase has been observed during boreal winter (Collimore et al., 2003; Liess & Geller, 2012; Son et al., 2017). In particular, the influence of the QBO cold phase on the convective systems of the MJO during boreal winter has been investigated in a number of recent studies (e.g., Liu et al., 2014; Nishimoto & Yoden, 2017; Yoo & Son, 2016). Lower temperatures and static stability at the tropopause in this season may allow for larger MJO amplitudes to occur during QBO cold phases.

The seasonality of the QBO-MJO relation found in previous studies is consistent with the seasonality of the QBO variations identified here. The zonal asymmetries of the QBO temperature signal are particularly pronounced during boreal winter and early spring (December–May, Figure 3). This time period overlaps with peaks in tropical overshooting convection during late winter and early spring (March–May; Liu & Zipser, 2005) and the seasonality of the QBO-MJO relation during winter (December–February) and extended winter (November–March). While for April and May no significant QBO-MJO relation has been detected (Yoo & Son, 2016), interaction between the QBO and convection could also be linked to other convective systems or convectively coupled waves. In particular, vertically propagating Kelvin waves in response to the convective heating can lead to colder temperatures above the regions of convection (Kim & Son, 2012).

In summary, QBO temperature variations in the TTL are not zonally symmetric. They show anomalously cold temperatures during QBO cold phases over regions associated with high-reaching convection during boreal winter and spring. Our analysis suggests a positive feedback mechanism where the QBO cold phase over convectively active regions leads to enhanced convection, thereby strengthening the cold phase temperature anomalies. While the observational evidence strongly supports the link between QBO zonal asymmetries and enhanced convective activities during QBO cold phases, further studies are needed to prove the causality of the mechanism.

Data Availability Statement

IGRA radiosonde data are available from https://www.ncdc.noaa.gov/data-access/weather-balloon/integrated-global-radiosonde-archive website. The GNSS-RO data are available upon registration from https://cdaac-www.cosmic.ucar.edu/cdaac/products.html website. Cloud top height data are available from https://bocachica.arc.nasa.gov/ website. Reanalyses fields used here are from the S-RIP common grid data files available at https://zenodo.org/record/3906864 website.

References

Baldwin, M. P., Gray, L. J., Dunkerton, T. J., Hamilton, K., Haynes, P. H., Randel, W. J., et al. (2001). The quasi-biennial oscillation. *Reviews of Geophysics*, *39*(2), 179–229. https://doi.org/10.1029/1999RG000073

Camargo, S. J., & Sobel, A. H. (2010). Revisiting the influence of the quasi-biennial oscillation on tropical cyclone activity. *Journal of Climate*, *23*, 5810–5825.

Collimore, C. C., Hitchman, M. H., & Martin, D. W. (1998). Is there a quasi-biennial oscillation in tropical convection? *Geophysical Reseasrch Letters*, *25*, 333–336.

Collimore, C. C., Martin, D. W., Hitchman, M. H., Huesmann, A., & Waliser, D. E. (2003). On the relationship between the QBO and tropical deep convection. *Journal of Climate*, *16*, 2552–2568. https://doi.org/10.1175/1520-0442(2003)

Davis, S. M., Liang, C. K., & Rosenlof, K. H. (2013). Interannual variability of tropical tropopause layer clouds. *Geophysical Research Letters*, *40*, 2862–2866. https://doi.org/10.1002/grl.50512

Dee, D. P., Uppala, S. M., Simmons, A. J., Berrisford, P., Poli, P., Kobayashi, S., et al. (2011). The ERA-Interim reanalysis: Configuration and performance of the data assimilation system. *Quarterly Journal of the Royal Meteorological Society*, *137*(656), 553–597. https://doi.org/10.1002/qj.828

Durre, I., Xungang, Y., Vose, R. L S., Applequist, S., & Arnfield, J. (2016). Integrated global radiosonde archive (IGRA) Version 2. *NOAA National Centers for Environmental Information*. https://doi.org/10.7289/V5X63K0Q [last access April 2020]

Efron, B., & Tibshirani, R. J. (1993). *An introduction to the bootstrap* (p. 436). New York: Chapman and Hall.

Emanuel, K. A. (1997). Some aspects of hurricane inner-core dynamics and energetics. *Journal of the Atmospheric Sciences*, *54*, 1014–1026.

Folkins, I. A., Loewenstein, M., Podolske, J., Oltmans, S., & Proffitt, M. (1999). A barrier to vertical mixing at 14 km in the tropics: Evidence from ozonesondes and aircraft measurements. *Journal of Geophysical Research*, *104*, 22,095–22,101.

Fueglistaler, S., Dessler, A. E., Dunkerton, T. J., Folkins, I., Fu, Q., & Mote, P. W. (2009). Tropical tropopause layer. *Reviews of Geophysics*, *47*, RG1004. https://doi.org/10.1029/2008RG000267

Fueglistaler, S., Haynes, P. H., & Forster, P. M. (2011). The annual cycle in lower stratospheric temperatures revisited. *Atmospheric Chemistry and Physics*, *11*, 3701–3711. https://doi.org/10.5194/acp-11-3701-2011

Gelaro, R., McCarty, W., Suárez, M. J., Todling, R., Molod, A., Takacs, L., et al. (2017). The Modern-Era Retrospective Analysis for Research and Applications, version 2 (MERRA-2). *Journal of Climate*, *30*(14), 5419–5454. https://doi.org/10.1175/JCLI-D-16-0758.1

Gettelman, A., Randel, W. J., Massie, S. T., Wu, F., Read, W., & Russell, J. (2001). El Niño as a natural experiment for studying the tropical tropopause region. *Journal of Climate*, *14*, 3375–3392.

Gettelman, A., Salby, M. L., & Sassi, F. (2002). Distribution and influence of convection in the tropical tropopause region. *Journal of Geophysical Research*, *107*(D10), 4080. https://doi.org/10.1029/2001JD001048

Giorgetta, M. A., Bengtsson, L., & Arpe, K. (1999). An investigation of QBO signals in the east Asian and Indian monsoon in GCM experiments. *Climate Dynamics*, *15*, 435–450.

Gray, W. M., Sheaffer, J. D., & Knaff, J. A. (1992). Hypothesized mechanism for stratospheric QBO influence on ENSO variability. *Geophysical Research Letters*, *19*, 107–110. https://doi.org/10.1029/91GL02950

Hamilton, K., Hertzog, A., Vial, F., & Stenchikov, G. (2004). Longitudinal variation of the stratospheric quasi-biennial oscillation. *Journal of the Atmospheric Sciences*, *61*(4), 383–402. https://doi.org/10.1175/1520-0469(2004)061<0383:lvotsq>2.0.co;2

Hersbach, H., de Rosnay, P., Bell, B., Schepers, D., Simmons, A., Abdalla, S., et al. (2018). *Operational global reanalysis: Progress, future directions and synergies with NWP*, *ERA Report Series* (Vol. 27).

Highwood, E. J., & Hoskins, B. J. (1998). The tropical tropopause. *Quarterly Journal of the Royal Meteorological Society*, *124*, 1579–1604. https://doi.org/10.1002/qj.49712454911

Holton, J. R., & Gettelman, A. (2001). Horizontal transport and the dehydration of the stratosphere. *Geophysical Research Letters*, *28*, 2799–2802.

Kiladis, G. N., Dias, J., Straub, K. H., Wheeler, M. C., Tulich, S. N., Kikuchi, K., et al. (2014). A comparison of OLR and circulation based indices for tracking the MJO. *Monthly Weather Review*, *142*, 1697–1715.

Kim, J., & Son, S. (2012). Tropical cold-point tropopause: Climatology, seasonal cycle, and intraseasonal variability derived from COSMIC GPS radio occultation measurements. *Journal of Climate*, *25*, 5343–5360. https://doi.org/10.1175/JCLI-D-11-00554.1

Knaff, J. A. (1993). Evidence of a stratospheric QBO modulation of tropical convection. Dept. of Atmospheric Science, Colorado State University, Fort Collins, CO, paper 520, p. 91

Kobayashi, S., Ota, Y., Harada, Y., Ebita, A., Moriya, M., Onoda, H., et al. (2015). The JRA-55 reanalysis: General specifications and basic characteristics. *Journal of the Meteorological Society of Japan*, *93*, 5–48. https://doi.org/10.2151/jmsj.2015-001

Liess, S., & Geller, M. A. (2012). On the relationship between QBO and distribution of tropical deep convection. *Journal of Geophysical Research*, *117*, D03108. https://doi.org/10.1029/2011JD016317

Liu, C., Tian, B., Li, K.-F., Manney, G. L., Livesey, N. J., Yung, Y. L., & Waliser, D. E. (2014). Northern Hemisphere mid-winter vortex-displacement and vortex-split stratospheric sudden warmings: Influence of the Madden-Julian Oscillation and Quasi-Biennial Oscillation. *Journal of Geophysical Research: Atmospheres*, *119*, 12,599–12,620. https://doi.org/10.1002/2014JD021876

Liu, C., & Zipser, E. J. (2005). Global distribution of convection penetrating the tropical tropopause. *Journal of Geophysical Research*, *110*, D23104. https://doi.org/10.1029/2005JD006063

Liu, N., & Liu, C. (2016). Global distribution of deep convection reaching tropopause in 1-year GPM observations. *Journal of Geophysical Research: Atmospheres*, *121*, 3824–3842. https://doi.org/10.1002/2015JD024430

Naujokat, B. (1986). An update of the observed quasi-biennial oscillation of the stratospheric winds over the tropics. *Journal of the Atmospheric Sciences*, *43*, 1873–1877.

Nishimoto, E., & Yoden, S. (2017). Influence of the stratospheric quasi-biennial oscillation on the Madden–Julian Oscillation during austral summer. *Journal of the Atmospheric Sciences*, *74*, 1105–1125. https://doi.org/10.1175/JAS-D-16-0205.1

Pan, L. L., Honomichl, S. B., Bui, T. V., Thornberry, T., Rollins, A., Hintsa, E., & Jensen, E. J. (2018). Lapse rate or cold point: The tropical tropopause identified by in situ trace gas measurements. *Geophysical Research Letters*, *45*, 10–756. https://doi.org/10.1029/2018GL079573

Patel, N., Sharma, S., Joshi, V., Kumar, P., Ojha, N., Kumar, K. N., et al. (2019). Observations of middle atmospheric seasonal variations and study of atmospheric oscillations at equatorial regions. *Journal of Atmospheric and Solar-Terrestrial Physics*, *193*, 105066. https://doi.org/10.1016/j.jastp.2019.105066

Pfister, L., Selkirk, H. B., Jensen, E. J., Schoeberl, M. R., Toon, O. B., Browell, E. V., et al. (2001). Aircraft observations of thin cirrus clouds near the tropical tropopause. *Journal of Geophysical Research*, *106*, 9765–9786. https://doi.org/10.1029/2000JD900648

Pilch Kedzierski, R., Matthes, K., & Bumke, K. (2020). New insights into Rossby wave packet properties in the extratropical UTLS using GNSS radio occultations. *Atmospheric Chemistry and Physics Discussions*, *20*(19), 11,569–11,592. https://doi.org/10.5194/acp-20-11569-2020

Plumb, R. A., & Bell, R. C. (1982). Equatorial waves in steady zonal shear flow. *Quarterly Journal of the Royal Meteorological Society*, *108*, 313–334. https://doi.org/10.1002/qj.49710845603

Randel, W. J., & Wu, F. (2015). Variability of zonal mean tropical temperatures derived from a decade of GPS radio occultation data. *Journal of the Atmospheric Sciences*, *72*, 1261–1275. https://doi.org/10.1175/JAS-D-14-0216.1

Saha, S., Moorthi, S., Pan, H. L., Wu, X., Wang, J., Nadiga, S., et al. (2010). The NCEP climate forecast system reanalysis. *Bulletin of the American Meteorological Society*, *91*(8), 1015–1058. https://doi.org/10.1175/2010BAMS3001.1

Solomon, S., Rosenlof, K. H., Portmann, R. W., Daniel, J. S., Davis, S. M., Sanford, T. J., & Plattner, G.-K. (2010). Contributions of stratospheric water vapor to decadal changes in the rate of global warming. *Science*, *327*(5970), 1219–1223. https://doi.org/10.1126/science.1182488

Son, S., Lim, Y., Yoo, C., Hendon, H. H., & Kim, J. (2017). Stratospheric control of the Madden–Julian Oscillation. *Journal of Climate*, *30*, 1909–1922. https://doi.org/10.1175/JCLI-D-16-0620.1

Tegtmeier, S., Anstey, J., Davis, S., Dragani, R., Harada, Y., Ivanciu, I., et al. (2020). Temperature and tropopause characteristics from reanalyses data in the tropical tropopause layer. *Atmospheric Chemistry and Physics*, *20*, 753–770. https://doi.org/10.5194/acp-20-753-2020

Thomason, L. W., Ernest, N., Millán, L., Rieger, L., Bourassa, A., Vernier, J.-P., et al. (2018). A global space-based stratospheric aerosol climatology: 1979–2016. *Earth System Science Data*, *10*, 469–492. https://doi.org/10.5194/essd-10-469-2018

Wallace, J. M., Panetta, R. L., & Estberg, J. (1993). Representation of the equatorial stratospheric quasi-biennial oscillation in EOF phase space. *Journal of the Atmospheric Sciences*, *50*, 1751–1762. https://doi.org/10.1175/1520-0469(1993)050<1751:ROTESQ>2.0.CO;2

Wang, J. S., Seidel, D. J., & Free, M. (2012). How well do we know recent climate trends at the tropical tropopause? *Journal of Geophysical Research*, *117*, D09118. https://doi.org/10.1029/2012JD017444

Yasunari, T. (1989). A possible lind of the QBOs between the stratosphere, troposphere and sea surface temperature in the tropics. *Journal of the Meteorological Society of Japan*, *67*, 483–493.

Yoo, C., & Son, S.-W. (2016). Modulation of the boreal wintertime Madden–Julian oscillation by the stratospheric quasi-biennial oscillation. *Geophysical Research Letters*, *43*, 1392–1398. https://doi.org/10.1002/2016GL067762

Yulaeva, E., & Wallace, J. M. (1994). The signature of ENSO in global temperature and precipitation fields derived from the microwave sounding unit. *Journal of Climate*, *7*, 1719–1736. https://doi.org/10.1175/1520-0442(1994)007<1719:TSOEIG>2.0.CO;2